TiMoCN based cermets. Part I. Morphology and phase composition

Daniele Mari, Stéphane Bolognini, Gilles Feusier, Thierry Cutard, Christian Verdon, Thomas Viatte, Willy Benoit

TiMoCN based cermets
Part I. Morphology and phase composition

D. Mari[a,*], S. Bolognini[a], G. Feusier[a], T. Cutard[a,1], C. Verdon[a,2], T. Viatte[b], W. Benoit[a]

[a]Departement de Physique, Institut de Physique de la Matière Complexe, Faculté des Sciences de Base, Ecole Polytechnique Fédérale Lausanne, CH-1015 Lausanne, Switzerland
[b]Allegheny Technologies, 1Teledyne Pl., LaVergne, TN 37086, USA

Cermets obtained by sintering powders of TiCN and Mo_2C with cobalt or nickel binder are studied in this paper. Different TiCN/Mo_2C ratios are used in order to vary the grain size. A characteristic core–rim structure of the ceramic phase is formed by precipitation of TiMoCN cubic carbide around undissolved TiCN cores. The morphological parameters of the materials such as grain size and the respective volume of rims and cores are determined by image analysis. The ceramic phase and the binder composition are measured by analytical scanning and transmission microscopy. The chemical composition of the phases, obtained after sintering, is modelled by a second order interface reaction controlled by molybdenum precipitation.

Keywords: Sintering; Image analysis; Molybdenum; Titanium carbonitride; Cobalt

1. Introduction

Composites made of transition metal carbides with a ferrous metal binder are widely used for cutting tool applications. Several families of such materials can be distinguished. WC–Co cemented carbides are the oldest and most widespread.

Hardmetals that are more refractory than WC–Co are found among those based on a TiC ceramic matrix and on TiMoCN carbides [1]. Such cermets have been mostly produced with a nickel binder but several successful attempts have been made to adopt a nickel–cobalt matrix [2–4]. Molybdenum is generally added as Mo_2C in the raw powders in order to obtain a good wetting of the ceramic by the metallic binder. Upon sintering, this compound gives rise to the formation of the characteristic core–rim structure of the TiMoCN grains [5,6]. It is today admitted that the rims are formed by solution precipitation of TiMoCN around the TiCN cores, which are the remainder of the original milled powder [7–9]. Ostwald ripening (OR) has been suggested to be the driving force of the rim growth [7] but the mechanism controlling the growth kinetics is still controversial, as diffusion controlled [6] or reaction controlled [7] growth are envisaged. Several authors [9–11] have suggested that two types of rims are formed during different stages of sintering: the so-called inner and outer rim. The inner rim should develop by chemical reaction of the TiCN and Mo_2C before the formation of the liquid phase, then the outer rim should be formed by precipitation of the carbides dissolved in the liquid metal [12].

Recent developments have shown that it is possible to control the sintering of TiCN–Mo based cermets with a cobalt binder [13]. These materials allow the combination of a tough cobalt binder with a refractory TiMoCN carbide skeleton. The aim of the present study is to investigate the relation between the morphology and the phase composition of TiCN–Mo–Co cermets. Different constituent parameters, namely the TiMoCN grain size and the cobalt content, are varied. An advanced morphological analysis of SEM images is performed in

* Corresponding author. Tel.: +41-21-693-4473; fax: +41-21-693-4470.
E-mail address: daniele.mari@epfl.ch (D. Mari).
[1] Present address: Ecole des Mines Albi-Carmaux, Centre des Matériaux, F-81000 Albi, France.
[2] Present address: ASULAB, 2074 Marin, Switzerland.

order to characterise the sintered structure. Cobalt and nickel based cermets are compared.

2. Materials and fabrication process

Two families of TiCN based material are considered in this study: the first one contains cobalt as a metal binder and the second one nickel. The composition of these materials is given in Table 1. Mo_2C is added in both families as a sintering aid. All samples are prepared with $TiC_{0.7}N_{0.3}$ which is shortened here as TiCN. During sintering, the Mo_2C is completely decomposed [1]. Part of the molybdenum enters the binder composition and the remainder of the Mo_2C contributes together with TiCN to the formation of the characteristic TiMoCN core–rim structure of the ceramic grains [6,10]. Different grain sizes are obtained both for TiCN–Mo–Co and TiCN–Mo–Ni by varying the molybdenum content: the higher the molybdenum content the smaller the grain size [14]. In the TiCN–Mo–Co family, the cobalt content is also changed while keeping constant the medium grain size obtained with 6.4 vol% Mo_2C.

Table 1
Composition and denomination of the different grades of this study

	TiCN	Mo_2C	Co
Composition TiCN–Mo–Co cermets [vol%]			
$TiMo_6Co_{13}$	80.6	6.4	13.0
$TiMo_6Co_{18}$	75.6	6.4	18.0
$TiMo_3Co_6$	90.4	3.2	6.4
$TiMo_6Co_6$	87.2	6.4	6.4
$TiMo_{13}Co_6$	80.6	13.0	6.4
Composition TiCN–Mo–Ni cermets [vol%]			
$TiMo_3Ni_6$	91.0	3.0	6.0
$TiMo_6Ni_6$	87.2	6.4	6.4
$TiMo_{13}Ni_6$	80.5	13.0	6.5

TiCN–Mo–Co and TiCN–Mo–Ni cermets are sintered at 1723 K under vacuum during the first hour and

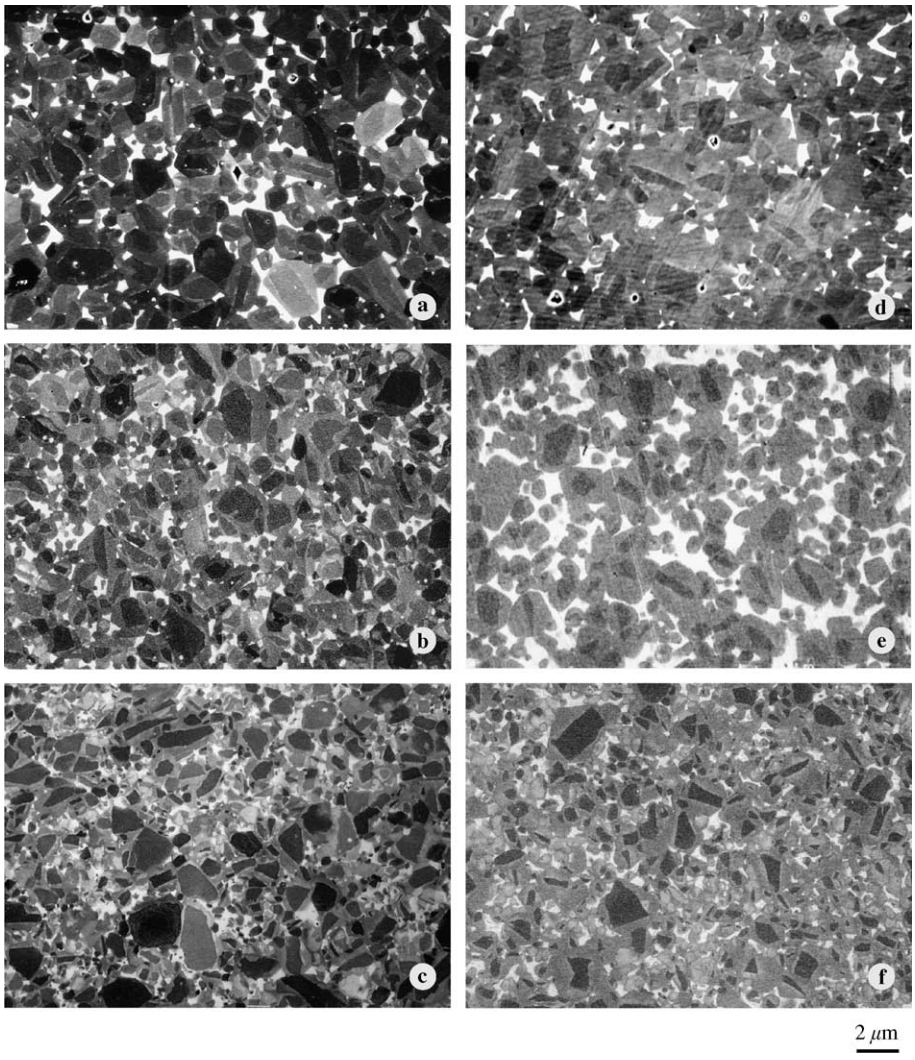

Fig. 1. SEM metallographic pictures of cermets: (a) $TiMo_3Ni_6$, (b) $TiMo_6Ni_6$, (c) $TiMo_{13}Ni_6$, (d) $TiMo_3Co_6$, (e) $TiMo_6Co_{18}$, and (f) $TiMo_{13}Co_6$. The same magnification is used in all images.

then HIPed during a second hour introducing argon at a pressure of 30 bar.

The morphology of the sintered samples, as observed by SEM, is shown in Fig. 1. The micrographs displayed in this figure are used for the image analysis described below.

3. Analysis techniques

3.1. Chemical analysis

The binder composition is analysed by EDS in TEM. Thin foils are prepared from spark-machined disks, mechanically ground down to 80 μm and ion milled to electron transparency. The field emission gun FEG-TEM used (Hitachi HF-2000) allows a lateral resolution better than 2 nm. TEM–EDS composition of the binder, reported in Table 2, is calculated considering the main metallic constituents: Ti, Mo and the metal binder. Each value given in Table 2 is the average composition of 16 different binder areas. The binder composition is found to be remarkably steady throughout the sample, as a result of the liquid sintering process. The ceramic grain composition is investigated both by TEM–EDS and by SEM–EDS. TEM–EDS line scans through whole TiCN grains have confirmed that the cores do not contain Mo whereas the rim exhibits a gradient of Mo concentration with a maximum close to the core–rim interface (inner rim). Moreover, the light boundary around cores, clearly seen in many grains of Fig. 1, indicates a local higher content of molybdenum. Therefore, a local measurement by TEM of Mo concentration in the rim does not reflect the average Mo content in the TiCN grains. In order to overcome this difficulty, EDS spectra were acquired by SEM over a large area (100×100 μm) on samples where the binder had been previously removed by chemical etching [15]. These measurements together with image analysis were used to establish the element partition in the material.

3.2. Image analysis: analysis of TiCN grain morphology

The analysis of carbonitride grains morphology is based on SEM micrographs taken for each grade. An automatic detection of the carbonitride grains is not possible as grain boundaries are not marked enough and contrast varies from a region to another of the same picture. To overcome this problem, phase boundaries are manually redrawn before analysis and specific grey levels are attributed to each phase. Detection and analysis of grains were performed with the software Concept VI 4.0 by Graftek used in a Labview environment. Each picture is analysed following the same procedure.

All the statistics are made on the same area of 320 μm^2. The volume fraction of each phase (binder, core and rim) is assessed on the basis of the measured surface fraction according to Underwood [16]. The grain size of the TiMoCN phase is calculated as $d = D\sqrt{3/2}$ where D is the projected grain size actually measured on images [16,17]. Due to the contour thickness of redrawn grains, the most reliable way to detect the volume fraction of phases resulted to be the detection of the binder fraction (see Table 3) which does not need grain redrawing. The volume fraction of TiMoCN grains is taken as the complement to the binder volume fraction.

The mean grain size $\bar{d}$ is calculated by fitting a Gaussian distribution of the logarithm of the grain size d, and taking the mean of the Gaussian curve so obtained [18]. The use of the logarithm is necessary to conserve only positive grain size.

The grain size distribution of TiMoCN grains (core + rim) for cobalt and nickel binder cermets are illustrated in Fig. 2. The grain sizes were grouped in classes of 0.1 μm to calculate statistical distributions. It is observed that the statistics are more scattered for large grain sizes due to the use of a constant sampling area. The comparison of grain size distributions is easier by using the statistical curves, which can be seen in Fig. 3a–c. The grain size seems to depend only on Mo content and remains remarkably stable when the Co content is varied.

Table 2
Results of EDS analysis

Sample	Mo at.% in binder	Ti at.% in binder	Co/Ni at.% in binder	Average Mo at.% in TiMoCN
$TiMo_6Co_{13}$	7.7 ± 0.8	2.8 ± 0.8	89.5 ± 1.6	8.7 ± 1.1
$TiMo_6Co_{18}$	6.9 ± 0.6	2.0 ± 0.4	91.1 ± 0.9	7.7 ± 1.0
$TiMo_3Co_6$	1.2 ± 0.6	2.5 ± 0.7	96.3 ± 1.2	5.0 ± 0.6
$TiMo_6Co_6$	10.1 ± 0.6	2.5 ± 0.4	87.4 ± 0.8	8.3 ± 1.2
$TiMo_{13}Co_6$	18.5 ± 2.8	2.1 ± 0.7	79.3 ± 4.7	15.1 ± 1.6
$TiMo_3Ni_6$	2.5 ± 0.4	7.5 ± 1.1	90.0 ± 1.3	3.3 ± 0.6
$TiMo_6Ni_6$	8.0 ± 0.6	7.5 ± 0.6	84.5 ± 1.3	7.6 ± 0.7
$TiMo_{13}Ni_6$	16.3 ± 0.3	5.6 ± 0.2	78.1 ± 0.4	16.0 ± 1.0

Atomic percentage of metal elements measured in the metal binder (TEM–EDS) and atomic percentage of molybdenum in the TiCN skeleton (SEM–EDS).

Table 3
Morphological parameters

	TiCN core size [μm]	TiMoCN grain (core + rim) size [μm]	Rim/core surface ratio	Binder volume [%]
TiMoCN–Co cermets				
$TiMo_6Co_{13}$	0.37	0.81	4.05	15.4
$TiMo_6Co_{18}$	0.38	0.76	4.96	17.1
$TiMo_3Co_6$	0.49	1.11	4.43	6.9
$TiMo_6Co_6$	0.38	0.85	3.18	6.6
$TiMo_{13}Co_6$	0.26	0.55	3.63	7.4
TiMoCN–Ni cermets				
$TiMo_3Ni_6$	0.39	0.71	1.94	7.9
$TiMo_6Ni_6$	0.28	0.58	2.50	8.8
$TiMo_{13}Ni_6$	0.22	0.46	1.91	7.2

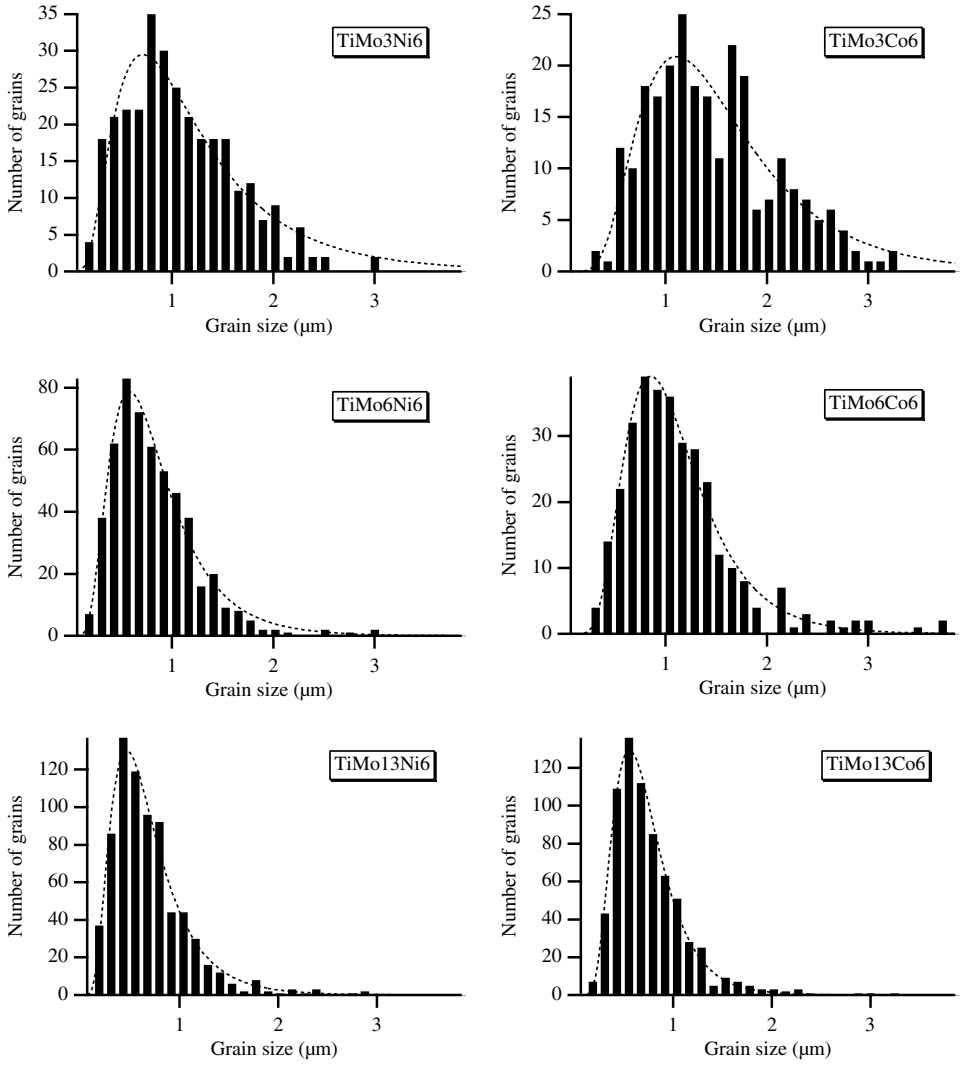

Fig. 2. Grain size distribution of different cermets. The fitted distribution, according to Eq. (1), is also shown (···).

However, the grain size distribution is broader in the case of cobalt binder samples. The core distribution is also calculated (Fig. 4a and b). One can observe that while small cores are preserved in small grain size samples (high molybdenum: $TiMo_{13}Co_6$, $TiMo_{13}Ni_6$), a significant amount of small cores is missing in large grain size

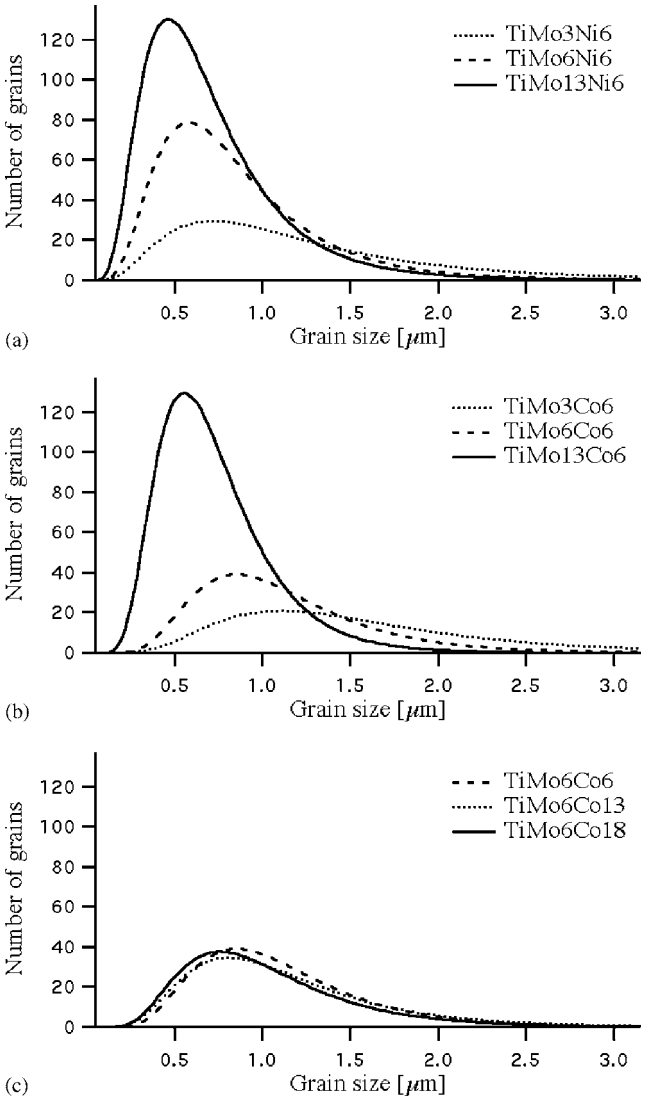

Fig. 3. Comparison of grain size distribution of different cermets as fitted by Eq. (1): (a) effect of Mo content in Ni-binder cermets, (b) effect of Mo content in Ni-binder cermets and (c) Co content does not affect the grain size distribution.

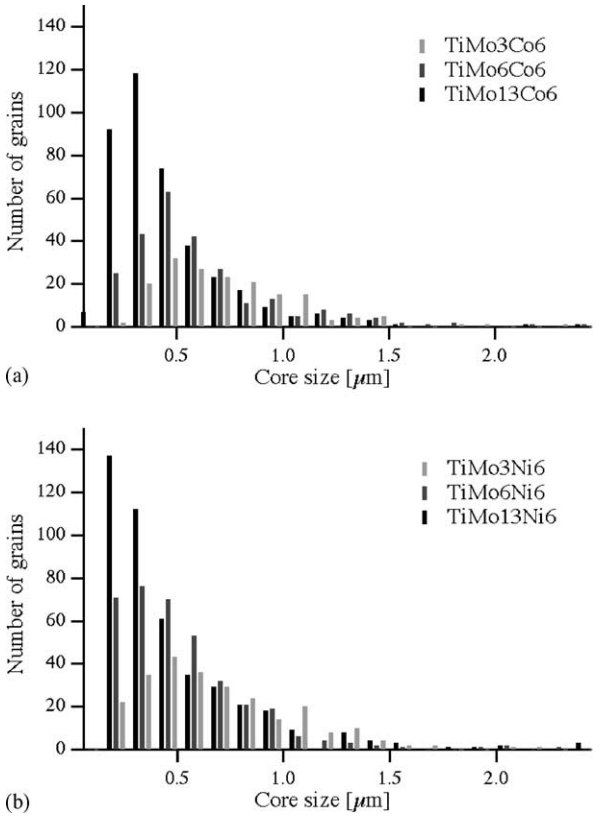

Fig. 4. TiCN core size distribution for (a) Co-binder and (b) Ni-binder cermets.

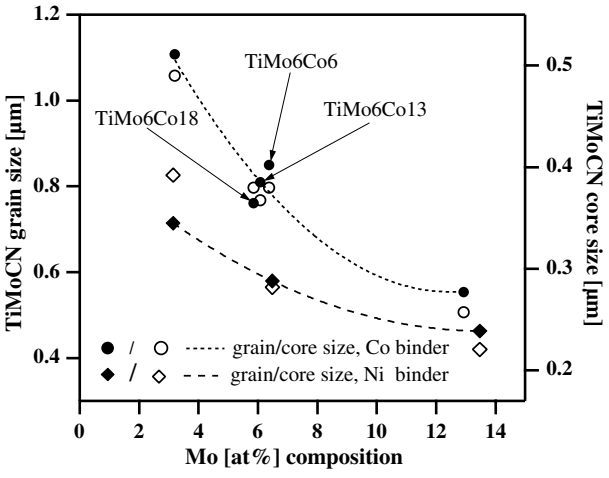

Fig. 5. Average grain size (core + rim) and core size of TiMoCN grains as a function of the Mo content in raw powders.

samples (low molybdenum). On the other hand, it is observed that, besides some statistical scatter, the core size distribution is almost equivalent in all grades for a core size larger than 0.7 μm. Finally, Ni-binder samples exhibit a smaller average core size (Table 3).

4. Discussion

4.1. Grain size distribution in cermets

The most important effect on the cermet morphology, observed when increasing the Mo content in raw powders, is a decrease in the final grain size of the carbonitride phase (Fig. 5). This effect may be explained by assuming that the molybdenum decreases the solubility of TiCN in the binder and so limits the grain growth by solution-precipitation during sintering. The solution of TiCN grains could be hindered by the formation of a Mo-rich shell, which is less soluble in the binder than pure TiCN and inhibits further solution of the carbonitride phase. A molybdenum-rich shell has been observed to form around TiCN grains by the authors and

Table 4
Molybdenum atom percent in carbonitride skeleton (balance is titanium)

	Mo measured in TiMoCN by SEM–EDS	Mo theoretical maximum in TiMoCN	Mo in TiMoCN balance with Mo in binder	Mo in TiMoCN rim	Mo in binder/Mo total
$TiMo_6Co_{13}$	8.7	7.7	5.5	6.7	0.30
$TiMo_6Co_{18}$	7.7	8.2	5.4	6.1	0.36
$TiMo_3Co_6$	5.0	3.6	3.5	4.2	0.04
$TiMo_6Co_6$	8.3	7.2	5.8	7.5	0.20
$TiMo_{13}Co_6$	15.1	14.5	12.0	14.8	0.20
$TiMo_3Ni_6$	3.3	3.5	3.2	4.8	0.09
$TiMo_6Ni_6$	7.6	7.3	6.2	9.4	0.15
$TiMo_{13}Ni_6$	16.0	15.2	13.0	16.2	0.17

The Mo balance content in the TiMoCN is calculated from Mo concentration in the binder measured by TEM–EDS (Table 1). Using the values in column 3, the atomic fraction in the rim is calculated from rim volume fraction with respect to TiCN grains (Eq. (A.5)). The ratio of Mo in the binder to total molybdenum is calculated according to Eq. (A.3).

was extensively studied by Lindahl et al. [4,9,19] who define it as the ''inner rim''. This hypothesis is supported by our study of the core distribution. The cores, that are composed of pure TiCN, can be considered as the remainder of the original milled TiCN powders [9]. If the precipitation of the Mo-rich shell before liquid phase sintering builds a barrier to the solution of TiCN grains in the liquid binder, then small cores should be more preserved in high-Mo grades (Fig. 4).

The formation of a chemical barrier to solution of the TiCN phase should considerably modify the growth kinetics and in particular the OR effect that has been envisaged for TiCN cermets [7]. In reality, the formation of the rim derives from the solution into the liquid binder of two compounds; TiCN and Mo_2C. Mo_2C is probably completely dissolved even before liquid phase sintering [4] and its precipitation is dictated by chemical equilibrium instead of interface energy minimisation like in the OR process. So, even if OR determines a driving force for large grains to grow at the expenses of small grains, the precipitation is probably controlled by equilibrium concentration of Ti and Mo in the binder and in the ceramic (see Section 4.2).

It is interesting to notice (Fig. 5) that the grain size and the core size distributions are very similar. This feature supports the hypothesis that the solubility of the ceramic phase in the binder controls the grain growth during sintering. In fact, if the average core size is high, it means that small cores have been dissolved and more material is available for rim formation, so leading to larger grains. According to this hypothesis, the larger size of grains found in Co-binder grades suggests that the solubility of TiCN in cobalt is higher than in nickel. This feature is also supported by the rim/core surface ratio measure (Table 3), which is generally higher in Co-binder samples.

4.2. Element partitioning in the phases of the cermets

The partition of the elements in the cobalt and in the carbide can deeply affect the mechanical properties of the cermets. As demonstrated by Cutard [20] in the case of Ni-binder cermets, the influence of the Mo distribution both in the ceramic and in the binder is a key to interpret the mechanical behaviour. In Table 4, the Mo content measured by SEM–EDS in the ceramic skeleton is compared with the theoretical maximum concentration. The SEM–EDS results generally give a molybdenum content in the rim which exceeds by 1–3 at.% the theoretical maximum content (see Table 4) calculated assuming that all the molybdenum goes into the rims. It should be considered that the error of EDS analysis is of the order of 1–2 at.% so that relatively small amounts of Mo cannot be assessed with enough precision. The overestimation of the Mo content can be explained by the error introduced by the analysis of a porous medium, as the one present in binder etched samples, while EDS measurement are based on the assumption of a homogeneous matrix. It is reasonable to believe that a too large quantity of molybdenum is detected, compared to the other elements, due to the fact that this metal is concentrated in rims, which are always close to holes from which X-rays can scatter more easily. Another way to determine the molybdenum content in the carbonitride grains is to calculate the balance with the binder content. First, the fraction of the molybdenum that is dissolved into the binder is measured by TEM–EDS (see Eq. (A.3) and Table 2). If no losses occur during sintering, the Mo balance must be contained in the TiCN grains. The values obtained (Table 4, column 4) do not exceed the maximum value expected from the base composition (column 2), which suggests that the TEM–EDS measurements in the binder are more reliable than those obtained by SEM–EDS. In the following analysis, we will only consider the molybdenum atom fractions obtained by TEM–EDS. The average atomic percent of Mo in the rim (Table 4, column 4) is calculated assuming that all the molybdenum present in TiCN grains is contained in the carbonitride rims and taking into account the rim/core ratio measured by image analysis.

It is interesting to plot the Mo content in the binder (Table 2) and in the rim (Table 4) as a function of the

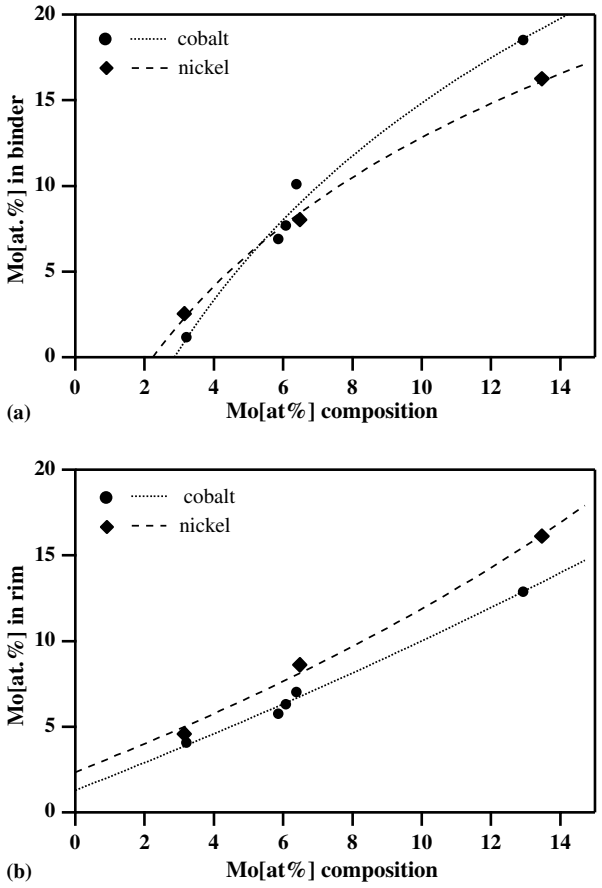

Fig. 6. Molybdenum atomic fraction in the binder (a) respectively in the rim (b) vs. the atomic fraction of Mo in raw powders. Experimental values are fitted according to Eq. (A.2) in (a) and to Eq. (A.3) in (b).

molybdenum content in raw powders (Fig. 6a and b). During the sintering, both TiCN and Mo_2C are dissolved into the liquid binder and precipitate as (Ti,-Mo)(C,N) which has a TiC cubic structure with Mo or N entering in substitutional position with respect to Ti or C. The dependence of Mo concentration in the rim from the initial Mo content rules out the hypothesis of a decomposition in two equilibrium phases: Co(Mo,Ti) and (Ti,Mo)(C,N). In such a case, as all sintering processes are made at the same temperature, one would expect the formation of two phases with constant composition and an increase of the rim volume as the Mo content increases. This is clearly not the case in our cermets (see Table 3, column 3). Nevertheless, the increase of the Mo concentration may be explained by chemical kinetics considerations. In a simple model, only Mo precipitation as Mo(C,N) can be considered assuming that, from the chemical kinetics point of view, the rate of reaction is independent on the Ti(C,N) concentration. If all the TiMoCN precipitates according to the Ti/C stoichiometric ratio, the reaction for Mo_2C precipitation from liquid binder is:

$$2\mathrm{Mo} + \mathrm{C} \rightarrow \mathrm{Mo} + \mathrm{MoC} \tag{1}$$

The kinetics of the reaction is determined by a nth order reaction according to the law (Appendix B):

$$-\frac{\mathrm{d}[\mathrm{Mo}_{\mathrm{binder}}]}{\mathrm{d}t} = k[\mathrm{Mo}_{\mathrm{binder}}]^n \tag{2}$$

As sintering goes on, the Mo concentration decreases in the cobalt. As demonstrated in Appendix B, the dependence of the average concentration $\overline{[\mathrm{Mo}_{\mathrm{binder}}]}$, at a fixed sintering time τ, on the initial concentration $[\mathrm{Mo}_{\mathrm{binder}}]_0$, is linear for a 1st order reaction and logarithmic for a 2nd order one. The convex shape curve of the Mo concentration in the binder (Fig. 6a) suggests a 2nd order reaction according to the law (Eq. (B.10)):

$$\overline{[\mathrm{Mo}_{\mathrm{binder}}]} = \frac{\ln(\kappa\tau[\mathrm{Mo}_{\mathrm{binder}}]_0 + 1)}{\kappa\tau} \tag{3}$$

Experimental data in Fig. 6a are fitted with an Eq. (4) slightly modified from Eq. (3):

$$\overline{[\mathrm{Mo}_{\mathrm{binder}}]} = \frac{\ln(\kappa\tau[\mathrm{Mo}_{\mathrm{powder}}]C_1 + 1)}{\kappa\tau} - \frac{C_2}{\kappa\tau} \tag{4}$$

$[\mathrm{Mo}_{\mathrm{powder}}]$ represents the concentration of molybdenum among metal elements entering the powder composition. The true initial concentration in the liquid binder $[\mathrm{Mo}_{\mathrm{binder}}]_0$ is not known precisely as it depends on the amount of titanium dissolved. It is assumed that $[\mathrm{Mo}_{\mathrm{binder}}]_0$ is proportional to the initial quantity of molybdenum and therefore the constant C_1 is introduced. Moreover, the plot in Fig. 6a seems to show a threshold composition close to 2.5 at.% Mo in the powders below which all the molybdenum precipitates into the rim. One more constant C_2 is introduced into (4) with respect to Eq. (B.10) to take into account this effect. The result of the fit is superimposed on measured concentrations (Fig. 6a). This approximation holds above the threshold concentration mentioned above. Below the threshold, there is no equilibrium saturation of the TiMoCN rim phase and all the molybdenum can precipitate in the ceramic. The presence of this threshold may be explained by the presence of an inner and an outer rim. The inner rim is probably formed already in the solid state [12] and immobilizes a certain amount of molybdenum corresponding to the threshold level. Then, the precipitation of the outer rim occurs in the liquid phase at equilibrium according to Eq. (2).

As also calculated in Appendix B, the precipitation rate of molybdenum into the rim and its average concentration can also be assessed. In this case, also considering a 2nd order reaction, the base equation derived from (B.14) is:

$$\overline{[\mathrm{Mo}_{\mathrm{rim}}]} = \frac{-\ln(1 - \kappa'\tau[\mathrm{Mo}_{\mathrm{powders}}]C_1')}{\kappa'\tau} + \frac{C_2'}{\kappa'\tau} \tag{5}$$

This law, which is the mirror of Eq. (4), fits correctly the values shown in Fig. 6b. The values of the fit parameters are reported in Table 5. Assuming a stoichiometric

Table 5
Fit parameters for the change of Mo concentration in the binder according to Eqs. (4) and (5)

Fit parameter	[Mo] in binder		[Mo] in the rim	
	Co-binder	Ni-binder	Co-binder	Ni-binder
$\kappa\tau/\kappa'\tau$	0.0485	0.0734	0.0203	0.0379
C_1/C_1'	5.000	5.000	0.800	0.800
C_2/C_2'	0.5136	0.6000	0.0259	0.0891

In Fig. 6a and b the fitted curves are plotted together with experimental data points.

concentration of carbon in TiCN powders, Eq. (1) implies that, if all the molybdenum precipitates into the rim, a carbon deficiency is obtained. Therefore, one can conclude that precipitation of the TiMoCN carbide can tolerate a certain carbon (or nitrogen) deficiency that is a well-known property of titanium carbides, nitrides and carbonitrides [21].

Together with the molybdenum concentration, the titanium concentration in the binder is also measured (see Table 2). It is interesting to notice that the concentration seems to depend essentially on the binder type and not on the relative amounts of constituents. The largest Ti contents are found in the nickel binder.

5. Conclusions

TiCN–Mo–Co/Ni cermets were sintered varying the binder and the molybdenum contents. The morphologies obtained after sintering were studied through SEM images and by different analytical methods such as EDS in TEM and SEM.

The effect of composition on the cermet morphology and chemistry is summarised as follows:

(1) After sintering, the carbide phase of the cermets exhibits the classical core–rim morphology. Grain growth is due to solution-precipitation of TiCN and Mo_2C. The molybdenum, introduced in the raw powders as Mo_2C, controls the TiMoCN grain growth. Precipitation first occurs in the inner rim, probably in the solid phase of the sintering. The precipitation in the outer rim occurs by a second order reaction controlled by the molybdenum equilibrium content.
(2) The molybdenum content reduces the carbide grain size. This effect is essentially due to the precipitation of the inner rim, which reduces dissolution of the TiCN particles.
(3) The Mo partition between the binder and the rim is a consequence of the C/N and Mo/Ti stoichiometry in the mixed carbide TiMoCN. The cobalt content has little influence on the grain size and the morphology. The titanium solubility depends almost exclusively on metal binder type. The solubility in Ni binder is higher than in the Co binder.

Acknowledgements

The authors would like to thank the support of Stellram SA (Gland, Switzerland) and the Commission pour la Technologie et l'Innovation which supported this work in project nos. 2495 and 3205.

Appendix A. Composition calculations

The atomic percent of molybdenum $Mo_{at.\%}$ (binder) in the binder, calculated considering metal species only, is given by:

$$[Mo_{binder}] = Mo_{at.\%}(binder) = \frac{Mo_{mol}(binder)}{Mo_{mol}(binder) + Ti_{mol}(binder) + Co, Ni_{mol}(binder)} \quad (A.1)$$

where Mo, Ti, Co,Ni_{mol} (binder) is the number of moles of Mo (respectively Ti or Co,Ni) in the binder.

From (A.1) one obtains:

$$Mo_{mol}(binder) = \frac{(Ti_{mol}(binder) + Co, Ni_{mol}(binder))Mo_{at.\%}(binder)}{1 - Mo_{at.\%}(binder)} \quad (A.2)$$

$Mo_{at.\%}$(binder) is given by the EDS measurements.

The fraction of molybdenum dissolved in the binder is simply given by:

$$Mo_{fract}(binder) = \frac{Mo_{mol}(binder)}{Mo_{mol}(total)} \quad (A.3)$$

The complementary fraction of molybdenum is supposed to be concentrated in the rim of carbonitride grains.

The molybdenum atomic percent calculated among metal species (Ti + Mo) in the rim can be obtained as follows:

$$[Mo_{rim}] = Mo_{at.\%}(rim) = \frac{Mo_{mol}(rim)}{Mo_{mol}(rim) + Ti_{mol}(rim)} \quad (A.4)$$

or

$$Mo_{at.\%}(rim) = \frac{1}{1 + \frac{Ti_{mol}(rim)}{Mo_{mol}(rim)}} \quad (A.5)$$

The titanium fraction in the rim can be calculated assuming that Mo has a substitutional character in the TiMoCN rim and therefore:

$$\frac{\mathrm{Mo_{mol}(rim)} + \mathrm{Ti_{mol}(rim)}}{\mathrm{Mo_{mol}(tot)} + \mathrm{Ti_{mol}(tot)}} = \frac{S_r}{S_{tot}} \tag{A.6}$$

where S_r/S_{tot} is the surface ratio between rims and grains and the subscript tot signifies the total amount of a species.

From (A.6) one obtains:

$$\frac{\mathrm{Ti_{mol}(rim)}}{\mathrm{Mo_{mol}(tot)} + \mathrm{Ti_{mol}(tot)}} = \frac{S_r}{S_{tot}} - \frac{\mathrm{Mo_{mol}(rim)}}{\mathrm{Mo_{mol}(tot)} + \mathrm{Ti_{mol}(tot)}} \tag{A.7}$$

The quantity $\mathrm{Mo_{mol}(rim)}/(\mathrm{Mo_{mol}(tot)} + \mathrm{Ti_{mol}(tot)})$ is obtained by EDS measurements.

By combining (A.7) and (A.5) the atomic fraction of molybdenum is calculated.

Appendix B. Reaction kinetics

Let us consider a simple chemical reaction:

$$n_a\mathrm{A} + n_b\mathrm{B} \Longleftrightarrow n_c\mathrm{C} + n_d\mathrm{D} \tag{B.1}$$

The rate of the reaction v is generally described by:

$$v = -\frac{1}{n_a}\frac{\mathrm{d[A]}}{\mathrm{d}t} = -\frac{1}{n_b}\frac{\mathrm{d[B]}}{\mathrm{d}t} = \frac{1}{n_c}\frac{\mathrm{d[C]}}{\mathrm{d}t} = \frac{1}{n_d}\frac{\mathrm{d[D]}}{\mathrm{d}t} \tag{B.2}$$

Where [A] indicates the concentration of A in a solvent (in our case the binder). The way the rate depends on concentration is generally described by:

$$v = \kappa[\mathrm{A}]^{\alpha}[\mathrm{B}]^{\beta} \tag{B.3}$$

Where α defines the order of the reaction with respect to A. κ is a constant. The rate of consumption of the component A is then:

$$v_A = -\frac{\mathrm{d[A]}}{\mathrm{d}t} = \kappa_a[\mathrm{A}]^{\alpha}[\mathrm{B}]^{\beta} \tag{B.4}$$

If the concentration of B is stoichiometric with respect to A, Eq. (B.4) can be simplified

$$v_A = -\frac{\mathrm{d[A]}}{\mathrm{d}t} = \kappa[\mathrm{A}]^{\alpha+\beta} \tag{B.5}$$

The order of the reaction is $\alpha + \beta$ and the consumption rate only depends on the concentration of A. In most chemical reactions, $\alpha = \beta = 1$ which makes them second order. By integrating Eq. (B.5) one obtains for a first order reaction ($\alpha + \beta = 1$):

$$[\mathrm{A}] = [\mathrm{A}]_0\,\mathrm{e}^{-\kappa t} \tag{B.6}$$

and for a second order reaction:

$$\frac{1}{[\mathrm{A}]} - \frac{1}{[\mathrm{A}]_0} = \kappa t \tag{B.7}$$

For a given reaction time τ, the average concentration $\overline{[\mathrm{A}]}$ can be calculated as:

$$\overline{[\mathrm{A}]} = \frac{1}{\tau}\int_0^{\tau}[\mathrm{A}]\,\mathrm{d}t \tag{B.8}$$

So, the decrease of $\overline{[\mathrm{A}]}$ in the solvent is given by:

$$\overline{[\mathrm{A}]} = \frac{[\mathrm{A}]_0}{\kappa\tau}(1 - \mathrm{e}^{-\kappa\tau}) \tag{B.9}$$

for a first order reaction and

$$\overline{[\mathrm{A}]} = \frac{\ln(\kappa\tau[\mathrm{A}]_0 + 1)}{\kappa\tau} \tag{B.10}$$

for a second order reaction. One can notice that increasing the initial concentration $[\mathrm{A}]_0$, the average concentration: $\overline{[\mathrm{A}]}$ increases linearly in first order reactions and logarithmically for second order reactions. However, for short times ($\kappa\tau \ll 1$) both reactions will give a linear dependence on the initial concentration:

$$\overline{[\mathrm{A}]} \approx [\mathrm{A}]_0$$

The precipitation kinetics of the product compounds C and D can be described in a similar way as for solute compounds considering the sign change in (B.2). The concentration of C vs. time will be defined by:

$$[\mathrm{C}] = [\mathrm{C}]_0\,\mathrm{e}^{+\kappa' t} \tag{B.11}$$

for a first order reaction and by:

$$\frac{1}{[\mathrm{C}]_0} - \frac{1}{[\mathrm{C}]} = \kappa' t \tag{B.12}$$

for a second order reaction. The reaction constant may be different and is named κ'. The average concentration $\overline{[\mathrm{C}]}$ for a given reaction time τ varies according to:

$$\overline{[\mathrm{C}]} = \frac{[\mathrm{C}]_0}{\kappa'\tau}(1 + e^{+\kappa'\tau}) \tag{B.13}$$

for a first order reaction and

$$\overline{[\mathrm{C}]} = \frac{-\ln(1 - \kappa'\tau[\mathrm{C}]_0)}{\kappa'\tau} \tag{B.14}$$

for a second order reaction.

References

[1] Doi H. Advanced TiC and TiC–TiN base cermets. In: Almond EA, Brookes CA, Warren R, editors. Science of hard materials. Bristol: Adam Hilger; 1986. p. 489–523.

[2] Pastor H. Etat Actuel et Développements des Matériaux Durs et Superdurs—Deuxième Partie. Matér Tech 1987;7–8:319–27.

[3] Pastor H. Titanium-carbonitride-based hard alloys for cutting tools. Mater Sci Engng A 1988;105–106:401–9.

[4] Andrén H-O, Rolander U, Lindahl PS. Phase composition in cemented carbides and cermets. Int J Refract Metals Hard Mater 1993–1994;12:107–13.

[5] Moskowitz D, Humenik M. Cemented titanium carbide cutting tools. In: Hausner HH, editor. Development and future prospects. New York: Plenum Press; 1966. p. 83–94.

[6] Chun DI, Kim DY. Microstructural evolution during the sintering of TiC–Mo–Ni cermets. J Am Ceram Soc 1993;76: 2049–52.

[7] Lindau L, Stjernberg KG. Grain growth in TiC–Ni–Mo and TiC–Ni–W cemented carbides. Powder Metall 1976;4:210–3.

[8] Yoshimura H, Sugisawa T, Nishigaki K, Doi H. Reaction during sintering of TiC–20TiN–15WC–10TaC–9Mo–5.5Ni–11Co cermet. Int J Refract Hard Met 1983;12:170–4.
[9] Lindahl P, Mainert T, Jonsson H, Andrén H-O. Microstructure and mechanical properties of a (Ti,W,Ta,Mo) (C,N)–(Co,Ni)-type cermet. J Hard Mater 1993;4:187–204.
[10] Suzuki H, Hayashi K, Terada O. Mechanisms of surrounding structure formation in sintered TiC–Mo_2C–Ni. Trans Jpn Inst Met 1971;35:936–42.
[11] Gee MG, Reece MJ, Roebuck B. High resolution electron microscopy of Ti(C,N) cermets. J Hard Mater 1992;3:119–42.
[12] Zackrisson J, Rolander U, Andrén H-O. Development of cermet microstructures during sintering. Metall Mater Trans A 2001; 32:85–94.
[13] Mari D, Bolognini S, Feusier G, Viatte T, Benoit W. Experimental strategy to study the mechanical behaviour of hardmetals for cutting tools. Int J Refract Metals Hard Mater 1999;17: 209–25.
[14] Viatte T. Propriétés Mécaniques à Haute Température des Cermets Ti(C,N)–Mo_2C–Ni Étudiés par Mesures de Frottement Intérieur et de Fluage, PhD thesis no. 1371. EPFL, Lausanne, 1995.
[15] Bolognini S, Feusier G, Mari D, Viatte T, Benoit W. High temperature mechanical behaviour of Ti(C,N)–Mo–Co cermets. Int J Refract Metals Hard Mater 1998;16:257–68.
[16] Underwood EE. The mathematical foundations of quantitative stereology. In: Pellissier GE, Purdy SM, editors. Stereology and quantitative metallography. Philadelphia: ASTM; 1972. p. 3–38.
[17] Viatte T et al. Investigation into the potential of a composite combining toughness and plastic deformation resistance. Int J Refract Metals Hard Mater 1999;17:79–89.
[18] Mendelson MI. Average grain size in polycrystalline ceramics. J Am Ceram Soc 1969;52:443–6.
[19] Lindahl P. Microstructure of Cermets, PhD thesis. Chalmers University of Technology, Göteborg, 1995.
[20] Cutard T, Viatte T, Feusier G, Benoit W. Microstructure and high temperature mechanical properties of $TiC_{0.7}N_{0.3}$–Mo_2C–Ni cermets. Mater Sci Eng 1996;A209:218–27.
[21] Schwarzkopf P, Kieffer R. Refractory hard metals. New York: The MacMillan Company; 1953.